Assessment of two vortex formulations for computing forces of a flapping foil at high Reynolds numbers

A. Martín-Alcántara and R. Fernandez-Feria
Fluid Mechanics, University of Málaga, Andalucía Tech, Dr Ortiz Ramos s/n, 29071 Málaga, Spain
(Dated: February 5, 2019)

Several vortex formulations for computing the lift and drag/thrust forces on a flapping foil are compared in terms of simplicity, accuracy and suitability for using with experimental data of measured velocity and vorticity fields. These methods are very useful to physically understand the aerodynamic performance of the flapping foil, and therefore the mechanisms of animal swimming and flight. In particular, we consider the case of a two-dimensional heaving foil at high Reynolds numbers and, using the results of accurate numerical simulations, we compare the performance of three force formulations based on the vortical impulse and Lamb's vector, projection of Lamb's vector, and wake integrals. We find that the formulation based on the vortical impulse is appropriate when all the vortices generated by the flapping foil remain close to the foil, such as in a starting motion or in hovering, but may become quite inaccurate for analyzing forward flight or swimming. In these later cases the projection method is much more appropriate because it only takes into account vorticity close to the moving solid body at each instant. In fact, we find that, for high Reynolds numbers, the performance of the projection method is always better, even in hovering, due to its simplicity and because it neatly separates the contribution of the added-mass force from the circulatory or vortical force component. Finally, it is shown that the standard integral momentum method, which is quite simple to implement in a forward motion using experimental data of the velocity field in the wake behind the solid body, is much less accurate than the methods based on vortex force formulas.

PACS numbers:

I. INTRODUCTION

Numerical modeling has become more and more important in studying the mechanisms of aquatic animal swimming and aerial animal flight, a central issue for developing robotics with good locomotion capability. To gain physical insight on these mechanisms, aerodynamic force formulas based on vortex dynamics have been proved to be particularly useful for analyzing the different components of the force exerted by the fluid on a solid moving through it [1–7]. This vortical approach is especially relevant in incompressible flows where, according to D'Alembert's paradox, vorticity is the only source of aerodynamic forces, discounting the added-mass force associated to the acceleration of the fluid caused by the moving solid body. Only incompressible flows will be considered here.

A vortical impulse theory was already used by von Kármán and Sears [8] to derive the lift and moment on an airfoil undergoing an arbitrary non-uniform motion in the inviscid and linear limit. For the case of an oscillating (flapping) airfoil, their results reproduced previous ones by Theodorsen [9], but providing new physical understanding about the different components of the lift force and moment based on the vorticity distribution. This linearized and inviscid vortical impulse theory has been recently extended to derive the thrust (or drag) force on a flapping airfoil [10].

A relevant generalization of the vortical impulse theory to viscous flows was developed by Wu [1]. Other significant contributions to the vortex force formulas used below were made by Quartapelle and Napolitano [11], Lighthill [2], Saffman [3], Chang [4], Howe [12], Noca et al. [5], and Wu et al. [6], among others. The application of some of these vortex formulas to the aerodynamic analysis of a flapping, two-dimensional (2D) airfoil has been recently made by several authors [13–16]. In the present work we compare some of these vortical formulations when applied to the heaving motion of a NACA0012 airfoil at high Reynolds numbers. This relatively simple flapping motion will allow for a critical assessment of the different vortex force formulas in terms of simplicity, accuracy and suitability for experimental or numerical data. In addition, this example will enable the characterization of the ranges of validity of the different approximations considered in the present work. In particular, we discuss general expressions for the aerodynamic force in a viscous incompressible flow which are written in terms of two of the most physically relevant vortex quantities employed to compute the aerodynamic force and moment: Lamb's vector, originally used by Prandtl in his vortex force (e.g., [3]), then appearing in the vortex projection formulas [4, 11, 12], and the vortical impulse, first introduced by Kelvin (e.g., [17]), and then used in more general expressions to compute hydrodynamic forces [1–3, 6].

The paper is organized as follows. In the next two sections the problem is formulated and the numerical

method is described and validated. The different vortex formulas for the aerodynamic forces are presented and simplified in section 4. The results from the different formulations are discussed in section 5, and some conclusions are drawn in the final section.

II. FORMULATION OF THE PROBLEM

We consider the two-dimensional (2D) and incompressible fluid motion generated by a foil (a NACA 0012) moving with constant horizontal speed U and vertical displacement given by

$$\hat{h} = \hat{h}_0 \cos(2\pi f \hat{t}) \tag{1}$$

through a fluid of density ρ and viscosity μ, where $\hat{h}_0$ is the amplitude and f the frequency of the foil's heaving motion. (The 'hat' symbol is used for dimensional quantities that will be used below in nondimensional form with the same letter.) In a reference frame with the origin attached to the foil's centroid (see Fig. 1), the nondimensional equations governing the fluid motion can be written as

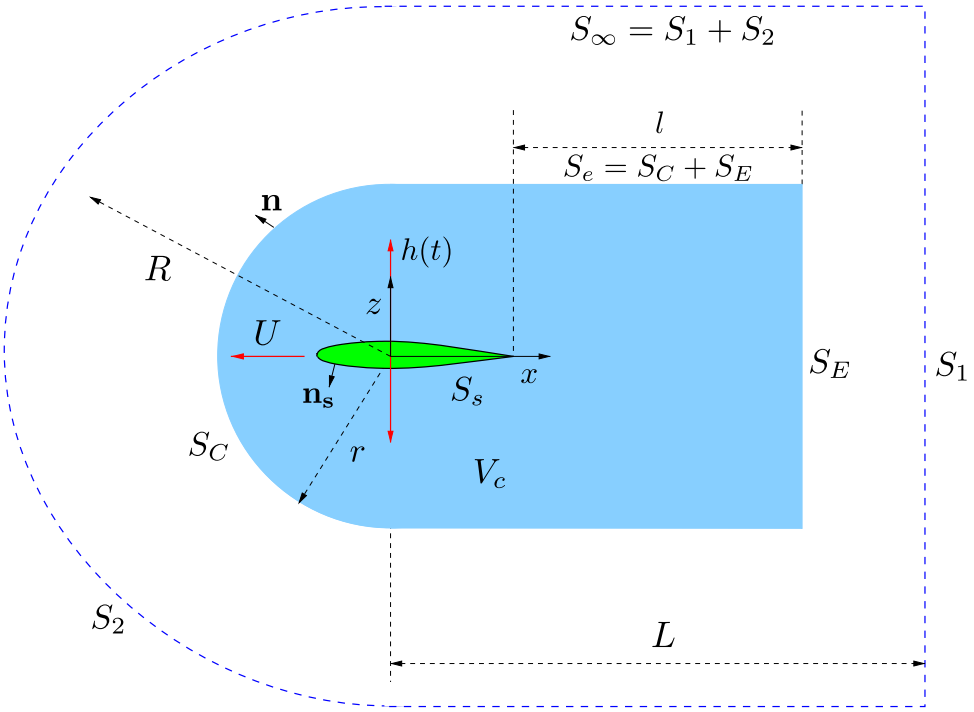

FIG. 1: Schematic of the heaving foil bounded by S_s, the integration domain delimited by the surfaces S_∞ and S_s, and the control volume V_c delimited by S_e and S_s.

$$\boldsymbol{\nabla}\cdot\mathbf{v} = 0\,, \qquad \frac{\partial \mathbf{v}}{\partial t} + \mathbf{v}\cdot\boldsymbol{\nabla}\mathbf{v} = -\boldsymbol{\nabla} p + \frac{1}{Re}\nabla^2\mathbf{v} - \frac{d\mathbf{V}}{dt}\,, \tag{2}$$

where the nondimensional coordinate $\mathbf{x} = (x, z)$ is scaled with the foil's chord length c, the fluid velocity $\mathbf{v}$ is scaled with U, time t with c/U, the pressure p (without the hydrostatic component) with ρU^2, and $Re = \rho c U/\mu$ is the Reynolds number. The last term in the momentum equation is due to the acceleration of the reference frame, where the nondimensional velocity $\mathbf{V}$ is given by

$$\mathbf{V} = -\mathbf{e}_x + \frac{dh}{dt}\mathbf{e}_z\,, \qquad h = h_0\cos(2kt)\,, \qquad k = \frac{\pi f c}{U}\,, \tag{3}$$

with $h = \hat{h}/c$, $h_0 = \hat{h}_0/c$ and k is the reduced frequency. Equations (2) for $\mathbf{v}$ and p have to be solved with suitable initial conditions and the following boundary conditions:

$$\mathbf{v} = \mathbf{0} \quad \text{on} \quad S_s\,, \qquad \mathbf{v} = -\mathbf{V} \quad \text{and} \quad p = 0 \quad \text{for} \quad |\mathbf{x}| \to \infty\,, \tag{4}$$

where S_s is the foil's surface (contour in 2D) oriented with normal $\mathbf{n}_s$ towards the fluid (see Fig. 1). Since the boundary conditions at infinity has to be implemented numerically on a finite surface S_∞ far from the foil, on part of this surface one has to modify the above boundary conditions to allow for the exit of the wake generated by the foil (see §III).

Once these equations are solved (see numerical method below), we are interested in the force (per unit length) exerted by the fluid on the foil, which in the present nondimensioal notation (the force per unit length is scaled with $\rho U^2 c$) is given by

$$\mathbf{F}(t) = -\int_{S_s} p\mathbf{n}_s dS + \frac{1}{Re}\int_{S_s} \boldsymbol{\omega} \wedge \mathbf{n}_s dS\,, \tag{5}$$

where $\boldsymbol{\omega} = \boldsymbol{\nabla} \wedge \mathbf{v} = \omega \mathbf{e}_y$ is the nondimensional vorticity (scaled with U/c). The $x-$ and $z-$ components of this force are the drag and lift coefficients, respectively. Actually, since these coefficients are traditionally defined as the corresponding force scaled with $\rho U^2 c/2$, one has to multiply by a factor of 2:

$$C_D(t) = 2\,\mathbf{F}\cdot\mathbf{e}_x\,, \qquad C_L(t) = 2\,\mathbf{F}\cdot\mathbf{e}_z\,. \tag{6}$$

For small amplitude of the oscillations, the flow and the corresponding force coefficients are periodic functions of time, with the period $T = \pi/k$ of the heaving motion. We designate time-averaged quantities over a cycle with an overbar; e.g.,

$$\overline{C}_D = \frac{1}{T}\int_{t_0}^{t_0+T} C_D(t)dt\,, \quad \overline{C}_L = \frac{1}{T}\int_{t_0}^{t_0+T} C_L(t)dt\,. \tag{7}$$

However, it is well known that for sufficiently large amplitudes and/or frequencies the flow is not longer periodic with period T, or becomes aperiodic [16, 18, 19]. The transitions are characterized by a Strouhal number which in the present notation is proportional to kh_0:

$$St = \frac{f2\hat{h}_0}{U} = \frac{2}{\pi}kh_0\,. \tag{8}$$

For these cases we shall also use time-averaged quantities over a cycle, but averaged in turn over a sufficiently large number N of cycles so that their values remain practically constant as N is increased [16]. These time-averaged quantities will be designated with $< \cdot >$; e.g.,

$$< C_D >= \frac{1}{NT}\int_{t_0}^{t_0+NT} C_D(t)dt\,, \quad < C_L >= \frac{1}{NT}\int_{t_0}^{t_0+NT} C_L(t)dt\,. \tag{9}$$

The mean values in these cases will be accompanied in the figures with error bars characterizing the standard deviations of the time-averaged values over a cycle. Obviously, for periodic flows, $\overline{\phi} =< \phi >$ for any quantity ϕ, and no error bars will be used.

We are mostly interested in cases in which $< C_D >$ is negative, so there is a net thrust force, with thrust coefficient $C_T = -C_D$. The propulsion efficiency is defined as

$$\eta = \frac{< C_T >}{< C_P >}\,, \tag{10}$$

where $< C_P >=< -C_L(dh/dt) >$ is the averaged input power coefficient, or power needed to heave the foil.

III. NUMERICAL METHOD AND VALIDATION

We solve numerically (2) with (4) in a C-shaped computational domain like that schematized in Fig. 1 using the open-source finite-volume code OpenFOAM [20].

The domain is delimited by the airfoil surface S_s and by an external surface $S_\infty = S_1 + S_2$ very far from the body, which consists of an upstream semicircular surface of nondimensional radius $R = 20$ attached to two parallel horizontal surfaces, one up and the other one down the foil (S_2), plus a downstream or exit surface S_1 perpendicular to the flight direction x, at a nondimensional distance $L = 20$ from the origin of coordinates. For the force formulas defined in §IV below we shall use a control volume V_c with the same shape as the integration domain, but smaller, delimited by the solid surface S_s and by a far surface $S_e = S_E + S_C$ (see Fig. 1).

Streamwise	Normal	Surface	#	t/T	$\max\{C_L\}$	$\lvert\varepsilon_r\rvert$	$< C_D >$	$\lvert\varepsilon_r\rvert$	rel. CPU time
541	61	189	74694	1000	11.44568	0.0030	0.20371	0.0600	0.14
1081	61	377	149506	1000	11.45195	0.0025	0.19923	0.0381	0.86
2161	61	753	299130	1000	11.48089	–	0.19191	–	–
541	121	189	150654	1000	11.44843	0.0011	0.20251	0.0568	0.05
1081	121	377	301546	1000	11.45959	0.0001	0.19569	0.0212	0.24
2161	121	753	603330	1000	11.46108	–	0.19162	–	–
1081	121	377	301546	500	11.48175	0.0019	0.19807	0.0072	0.88
1081	241	377	605626	1000	11.45987	–	0.19665	–	–
1081	121	377	301546	2000	11.46155	0.0001	0.19572	0.0047	1.5

TABLE I: Numerical convergence analysis in terms of the maximum value of C_L and $< C_D >$ (sixth and eighth columns, respectively), with the corresponding relative error $|\varepsilon_r|$ in their respective right hand side column, for $h_0 = 0.05$, $k = 6$ and $Re = 20\,000$. The first three columns show the number of cells in the streamwise direction, normal direction, and around the foil, respectively, with the total number given in the fourth column. The fifth column shows the temporal resolution as the number of time steps per cycle of period T. The last column shows the fraction of CPU time per cycle in relation to the case marked with a dash.

As boundary conditions we use $\mathbf{v} = \mathbf{0}$ on S_s, $\mathbf{v} = -\mathbf{V}$ on S_2, and $\mathbf{n} \cdot \boldsymbol{\nabla}\mathbf{v} = \mathbf{0}$ and $p = 0$ on S_1, where $\mathbf{n}$ is the unit vector normal to the surfaces pointing out of the integration volume.

For the spatial discretization we use a second order, Gauss Linear upwind differencing scheme [20, 21]. This scheme employs upwind interpolation weights, with an explicit correction based on the local cell gradient, which is a stable and accurate choice when dealing with convective-dominated flows. On the other hand, time is advanced by half-blending a second order Crank-Nicolson scheme with implicit Euler integration, to ensure boundedness. Moreover, the pressure-velocity coupling is treated through the Semi-Implicit Method for Pressure Linked Equations (SIMPLE) algorithm [22], which allows to advance in time with CFL > 1 [23, 24]. Finally, the integrals to compute the different force components are discretized with second-order accuracy by using the midpoint rule in combination with linear interpolation schemes [16].

To validate the numerical method we compare with several available experimental and numerical results for heaving foils, after performing a grid convergence analysis whose results are shown in Table I. We vary both, the spatial resolution (top six rows in Table I), and the temporal resolution (last three rows). We finally chose the same grid resolution as Young and Lai [25], i.e. $1081 \times 121 \times 377$, in the streamwise direction, normal direction, and around the foil, respectively. Though there is hardly any difference in the force coefficients for any of the grid resolutions (see Table I), the selected spatial density ensures enough accuracy in the wake behind the foil to properly solve the integrals along S_E. The first normal grid point on the airfoil surface is located at 9.2×10^{-5}, which reproduces the vortex shedding occurring for a steady foil at $Re = 20\,000$ [25]. The time step in all the cases was chosen such that the number of time steps within one period was 1000, half of the one employed by Bos et al. [24] for hovering motion, and in contrast to Lian and Shyy [23], who set this ratio to be 100. Ratios of 2000 and 500 time steps per period were also tested, obtaining no differences in the results (see Table I).

For the first validation case we choose the experimental data of McGowan et al. [26] for the lift coefficient of a heaving foil at $Re = 10\,000$, $h_0 = 0.025$ and $k = 7.86$ (Fig. 2). The numerical results, which are strictly periodic for this small value of $kh_0 \simeq 0.2$, practically coincide with the theoretical results by Theodorsen and agree quite well with the experimental results.

As the second validation case we select the experimental results of Heathcote and Gursul [27] for the time-averaged thrust coefficient and propulsion efficiency of a heaving NACA 0012 airfoil in the range $0 \leq k \leq 6.3$, for $h_0 = 0.175$ and several Reynolds numbers. Figures 3 and 4 compare these experimental results with our numerical results for $Re = 20\,000$, and the numerical results by Young and Lai [25] for the same Reynolds and h_0. Our present numerical results cease to be periodic with period T for $kh_0 \gtrsim 0.3$, as marked with a shaded zone and with the corresponding error bars in both figures. Also shown in Figs. 3-4 are the theoretical results by Garrick [28] and Fernandez-Feria [10] (see also §IV B below), both corrected with the quasi-static averaged thrust C_{T0} computed numerically as $k \to 0$ for the same Re and h_0 [29, 30] (C_{T0} is obviously negative, i.e., a drag coefficient, and in the present case is quite small, $C_{T0} \simeq -0.028$). In this work, all the simulations with $kh_0 > 0$ are started from the periodic vortex shedding solution appearing in the steady case ($kh_0 = 0$).

The experimental and numerical results agree quite well in all the range of values of k considered, with a larger discrepancy for $kh_0 \gg 0.3$, obviously due to the oscillations in the averaged computational values associated to the chaotic behavior of the solution, that become a relevant fraction of the mean values for large kh_0. Another interesting feature of Fig. 3 is that the theoretical results by Fernandez-Feria agree quite well

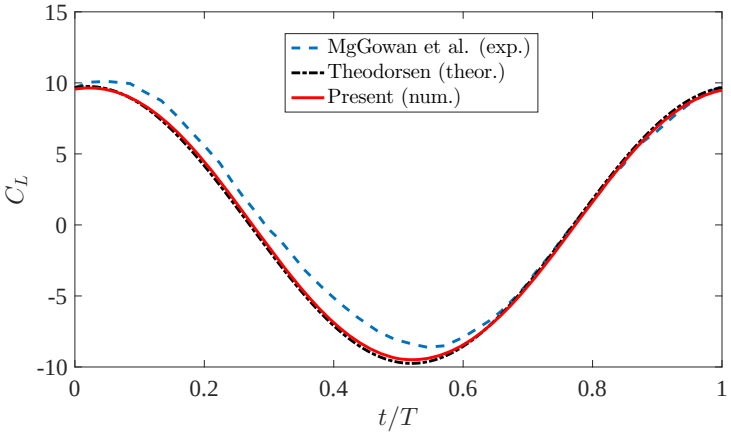

FIG. 2: $C_L(t)$ during a cycle computed for $Re = 10\,000$, $h_0 = 0.025$ and $k = 7.86$ compared with the experimental results of McGowan et al. [26] and the theoretical ones by Theodorsen [9].

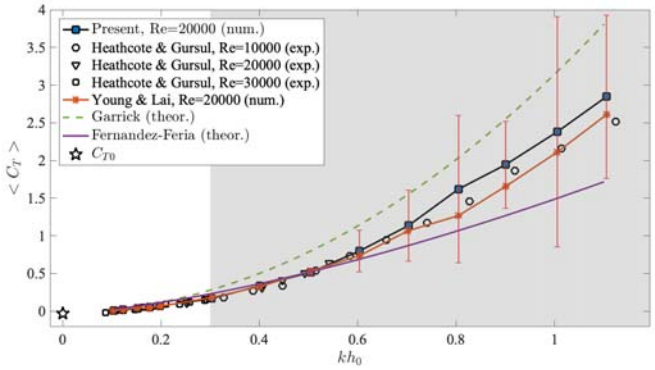

FIG. 3: Averaged C_T vs. kh_0 computed for $h_0 = 0.175$ and $Re = 20\,000$ compared with experimental results of Heathcote and Gursul [27] for the same values of h_0 and k and three Reynolds number, and the numerical results by Young and Lai [25] for the same conditions. Also included are the theoretical results by Garrick [28] and Fernandez-Feria [10], both corrected with $C_{T0} \simeq -0.028$. The shaded area corresponds to the values of kh_0 for which our numerical results are not longer periodic with period T, and error bars are included for the present numerical results.

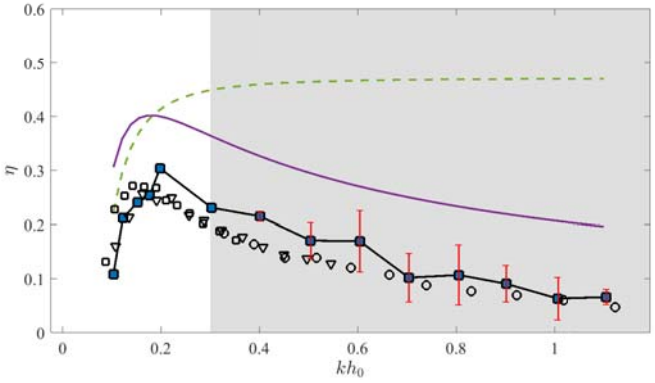

FIG. 4: η vs. kh_0 for the same cases plotted in Fig. 3, except the numerical results by Young and Lai (same legend).

with the experimental and numerical results up to $kh_0 \simeq 0.5$ ($St \simeq 0.32$), i.e., while the solution is periodic, or the oscillations in the averaged values due to the aperiodicity of the flow remain sufficiently small.

IV. SUMMARY OF SOME FORCE FORMULAS FOR TWO DIMENSIONAL AND INCOMPRESSIBLE FLOWS

In all the force formulations described below, the control volume V_c is that depicted in Fig. 1, bounded by the foil surface S_s and by $S_e = S_C + S_E$. The semicircular part of S_C is located at a nondimensional radius $r = 10$ (see Fig. 1), while the downstream surface S_E is located at a variable distance l from the trailing edge of the airfoil to analyze the effect of the exit wake on the different force formulas.

A. Vortex force

It is well known (see, e.g., [3]) that for an incompressible and steady flow at high Reynolds numbers, when the flow is irrotational on the surface S_e far from the solid body, the force on the surface S_s of the body can be written in terms of an integral of Lamb's vector $\boldsymbol{\mathcal{L}} = \boldsymbol{\omega} \wedge \mathbf{v}$ over the control volume V_c. This is sometimes called the vortex force. (Note that here we use the nondimensional Lamb's vector $\boldsymbol{\mathcal{L}}$, which is scaled with U^2/c)

More generally, but for an *incompressible and two dimensional flow*, the nondimensional force $\mathbf{F}$ on the solid V_s bounded by S_s can be written as [31]:

$$\mathbf{F} = -\int_{V_c} \boldsymbol{\mathcal{L}} dV - \int_V \mathbf{x} \wedge \frac{\partial \boldsymbol{\omega}}{\partial t} dV - \int_{S_e} \mathbf{x} \wedge (\mathbf{n} \wedge \boldsymbol{\mathcal{L}})\, dS + \int_{V_s} \frac{\partial}{\partial t}(\mathbf{v} + \mathbf{V}) dV + \int_{S_s} \frac{v^2}{2} \mathbf{n}_s dS +$$

$$+ \frac{1}{Re} \int_{S_e} \left[\boldsymbol{\omega} \wedge \mathbf{n} - \mathbf{x} \wedge (\mathbf{n} \wedge \boldsymbol{\nabla} \wedge \boldsymbol{\omega})\right] dS\,, \tag{11}$$

where $V = V_c + V_s$. Note that all the quantities are dimensionless, and that the terms integrated over the solid body (V_s and S_s) are written in a different, but equivalent, form to J.-Z. Wu et al. [31].

For high Reynolds number one may neglect the last term integrated over S_e. Also, the other integral over S_e is negligible except on S_E, because far from the body vorticity is only present in the wake exiting V_c through S_E. Since the flow is 2D and referred to a frame moving with the foil,

$$\boldsymbol{\mathcal{L}} = \boldsymbol{\omega} \wedge \mathbf{v} = \omega(v_z \mathbf{e}_x - v_x \mathbf{e}_z)\,, \tag{12}$$

and $\mathbf{v} = \mathbf{0}$ in V_s (and on S_s). Thus, (11) can be written as

$$\mathbf{F} \simeq \mathbf{F}_v + \mathbf{F}_I + \mathbf{F}_{oE} + \mathbf{F}_V\,, \tag{13}$$

with

$$\mathbf{F}_v = -\int_{V_c} \boldsymbol{\mathcal{L}} dV = \int_{V_c} \omega(-v_z \mathbf{e}_x + v_x \mathbf{e}_z) dV\,, \tag{14}$$

$$\mathbf{F}_I = -\int_V \mathbf{x} \wedge \frac{\partial \boldsymbol{\omega}}{\partial t} dV = \int_V \frac{\partial \omega}{\partial t}(z \mathbf{e}_x - x \mathbf{e}_z) dV\,, \tag{15}$$

$$\mathbf{F}_{oE} = -\int_{S_E} \mathbf{x} \wedge (\mathbf{n} \wedge \boldsymbol{\mathcal{L}})\, dS = \int_{S_E} v_x \omega (z \mathbf{e}_x - x \mathbf{e}_z) dz\,, \tag{16}$$

$$\mathbf{F}_V = \frac{d}{dt} \int_{V_s} \mathbf{V} dV = V_s \frac{d^2 h}{dt^2} \mathbf{e}_z\,. \tag{17}$$

The notation $\mathbf{F}_I$, with the subscript I for 'impulse', will be clear in §IV B below. The last term $\mathbf{F}_V$, integrated over the volume of the foil V_s, and which only contributes to the vertical force in the present case, is usually very small because the nondimensional volume (actually area, scaled with c^2) of the NACA 0012 foil is $V_s \simeq 0.11$. Only for sufficiently high reduced frequencies this term can be relevant. For a stationary flow and neglecting the vorticity exiting V_c through S_E (when V_c is practically unbounded) one recovers the vortex force $\mathbf{F} \simeq \mathbf{F}_v$ [3].

B. Vortical impulse

The vortical impulse theory to compute the unsteady force and moment exerted by a fluid on a solid body was formulated in general terms by J. C. Wu [1], though the connection between the variation of the impulse and the fluid forces was already well known for some particular cases (e.g., [2, 17, 32]). For an incompressible and two dimensional flow it can be written, in nondimensional form, as

$$\mathbf{F} = -\frac{d\mathbf{I}}{dt} + \frac{d}{dt}\int_{V_s} (\mathbf{v}+\mathbf{V})dV\,, \qquad \mathbf{I} = \int_{V_\infty} \mathbf{x}\wedge\boldsymbol{\omega} dV\,, \tag{18}$$

where V_∞ is the entire unbounded volume, including the solid volume V_s, and the nondimensional impulse $\mathbf{I}$ is scaled with c^2U. This general and elegant expression has the drawback that it cannot be used in practical cases where the velocity and vorticity fields are computed numerically, or obtained experimentally, in a finite volume such as V_c in Fig. 1. However, it is the base for some interesting theoretical formulations like the linearized potential theory for very thin airfoils [8, 10], for which the second term of $\mathbf{F}$ in (18) becomes negligible. The theoretical expressions for C_L and C_T used in Figs. 2-4 above (except that of Garrick) are based in this formulation, though the results for C_L where previously derived by Theodorsen [9] from standard potential theory. Thus, the results from the linearized potential theory can be seen as the limit of (18) when $Re\to\infty$ for very thin airfoils where $V_s\to 0$.

For a finite volume like V_c depicted in Fig. 1, one may generalize (18) for $\mathbf{I}_V$ defined in the finite volume $V = V_c + V_s$, instead of the unbounded volume V_∞,

$$\mathbf{I}_V = \int_V \mathbf{x}\wedge\boldsymbol{\omega} dV\,, \tag{19}$$

by using (11). In fact, since V is a stationary volume in the present reference frame,

$$-\frac{d\mathbf{I}_V}{dt} = -\frac{d}{dt}\int_V \mathbf{x}\wedge\boldsymbol{\omega} dV = -\int_V \mathbf{x}\wedge\frac{\partial\boldsymbol{\omega}}{\partial t}dV = \mathbf{F}_I \tag{20}$$

is the term defined in (15), so that (11), or (13), is a generalization of (18) for a finite volume. In particular, the expression (13) contains two additional terms in relation to (18), $\mathbf{F}_v$, or the vortex force, that vanishes for an unbounded volume [6], and $\mathbf{F}_{oE}$, which also vanishes as S_E is pushed to infinity.

C. Projection formulas

One of the main disadvantages of the above force expressions in terms of the vortical impulse and Lamb's vector is that vorticity far from the body, and/or inside the thin boundary layer on the surface of the body for high Reynolds numbers, may contribute very significantly to the aerodynamic force, making often quite difficult to apply them to practical cases where the vorticity and velocity fields are obtained experimentally or numerically. One way to circumvent this difficulty is by using projection functions that satisfy Laplace's equation and appropriate boundary conditions [4, 11, 12]. We shall use here the formulation due to Chang [4], which has been proved to be quite useful to understand the forces on a heaving and pitching foil [16, 33] in terms of the vorticity distribution in the vicinity of the foil.

For an incompresible flow, the nondimensional force on S_s can be written as

$$\mathbf{F} = -\int_{S_s} dS\,\mathbf{n}_s\cdot\frac{\partial}{\partial t}(\mathbf{v}+\mathbf{V})\boldsymbol{\varphi} + \int_{S_s}\frac{v^2}{2}\mathbf{n}_s dS + \int_{V_c}\boldsymbol{\mathcal{L}}\cdot\boldsymbol{\nabla}\boldsymbol{\varphi} dV + \frac{1}{Re}\int_{S_s}(\boldsymbol{\omega}\wedge\mathbf{n}_s)\cdot(\mathsf{I}+\boldsymbol{\nabla}\boldsymbol{\varphi})\,dS\,, \tag{21}$$

where the auxiliary vector function $\boldsymbol{\varphi} = \varphi_x\mathbf{e}_x + \varphi_z\mathbf{e}_z$ satisfies

$$\nabla^2\boldsymbol{\varphi} = \mathbf{0}\,, \quad \mathbf{n}_s\cdot\boldsymbol{\nabla}\boldsymbol{\varphi} = -\mathbf{n}_s \quad \text{on } S_s\,, \tag{22}$$

and I is the unit tensor. Actually, since the components of $-\boldsymbol{\varphi}$ coincide with the translational potentials defining the added-mass coefficients associated to the acceleration $d\mathbf{V}/dt$ in a potential flow (see, e.g., [34]), and since the foil does not rotate in the present case ($\mathbf{v}=\mathbf{0}$ on S_s), the first term in (21) can be written as

$$-\frac{d\mathbf{V}}{dt}\cdot\int_{S_s}\mathbf{n}_s\boldsymbol{\varphi}\,dS = -\frac{d\mathbf{V}}{dt}\cdot\int_{S_s}\frac{\partial\boldsymbol{\varphi}}{\partial n}\boldsymbol{\varphi}\,dS = -\mathsf{m}\cdot\frac{d\mathbf{V}}{dt}\,, \tag{23}$$

where $\mathsf{m} = \int_{S_s} \boldsymbol{\varphi}(\partial\boldsymbol{\varphi}/\partial n)dS$ is the nondimensional added-mass tensor (scaled with ρc^2), with $\mathbf{n} = -\mathbf{n}_s$ being the unit vector normal to S_s pointing towards the interior of the body. (Actually, m is the part of the 6×6 added-mass tensor corresponding to the 2D translational acceleration.)

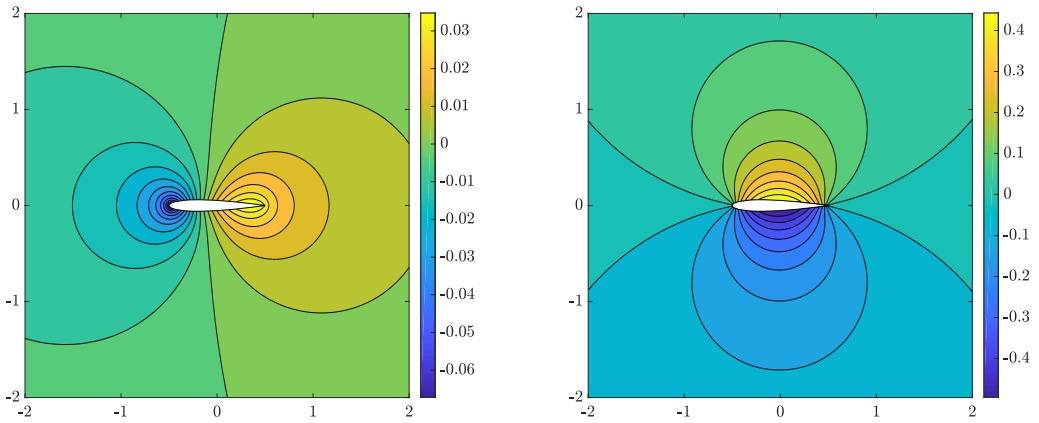

FIG. 5: Functions $\varphi_x(x,z)$ (left) and $\varphi_z(x,z)$ (right) for a NACA 0012 foil.

Neglecting the last term of (21) for high Reynolds numbers, and taking into account that the second term vanishes because $\mathbf{v} = \mathbf{0}$ on S_s in the present reference frame, the force can be simply written as the sum of an added-mass term and a vortical component given by the volume integral of Lamb's vector conveniently projected:

$$\mathbf{F} \simeq \mathbf{F}_{am} + \mathbf{F}_{vf}\,, \tag{24}$$

with

$$\mathbf{F}_{am} = -\mathsf{m} \cdot \frac{d\mathbf{V}}{dt} = -m_{xz}\frac{d^2h}{dt^2}\mathbf{e}_x - m_{zz}\frac{d^2h}{dt^2}\mathbf{e}_z\,, \tag{25}$$

$$\mathbf{F}_{vf} = \int_{V_c} \boldsymbol{\mathcal{L}} \cdot \boldsymbol{\nabla}\boldsymbol{\varphi} dV = \int_{V_c} \omega \left[\left(v_z\frac{\partial\varphi_x}{\partial x} - v_x\frac{\partial\varphi_x}{\partial z}\right)\mathbf{e}_x + \left(v_z\frac{\partial\varphi_z}{\partial x} - v_x\frac{\partial\varphi_z}{\partial z}\right)\mathbf{e}_z\right] dV\,. \tag{26}$$

Figure 5 shows the auxiliary potential functions φ_x and φ_z for a NACA 0012 foil computed by solving numerically (22). From them it is found that $m_{xz} = 0$ and $m_{zz} = 0.769232$ (these values may be compared with the theoretical ones for a flat plate, 0 and $\pi/4$, respectively [34]), so that the x component in the added-mass force (25) vanishes, and the only contribution to the force in the direction of flight comes from the vortex, or circulatory, force (26).

D. Integral momentum

Finally, as a standard reference we shall use the expression of the force computed from the integral momentum theorem applied to the control volume V_c. Assuming that viscous forces are negligible on the surface S_e [just like in previous expressions (13) and (24)], that the pressure is constant on S_e, that $\mathbf{v} = -\mathbf{V}$ on the part S_C of this surface S_e, and using mass conservation, the nondimensional force on S_s can be written as

$$\mathbf{F} \simeq \mathbf{F}_{tv} + \mathbf{F}_{vE}\,, \tag{27}$$

where

$$\mathbf{F}_{tv} = -\frac{d}{dt}\int_{V_c}(\mathbf{v}+\mathbf{V})dV = -\frac{d}{dt}\int_{V_c}\left[v_x\mathbf{e}_x + \left(v_z + \frac{dh}{dt}\right)\mathbf{e}_z\right]dV\,, \tag{28}$$

$$\mathbf{F}_{vE} = -\int_{S_E}(\mathbf{v}+\mathbf{V})v_x dS = -\int_{S_E}\left[(v_x - U)v_x\mathbf{e}_x + \left(v_z + \frac{dh}{dt}\right)v_x\mathbf{e}_z\right]dS\,. \tag{29}$$

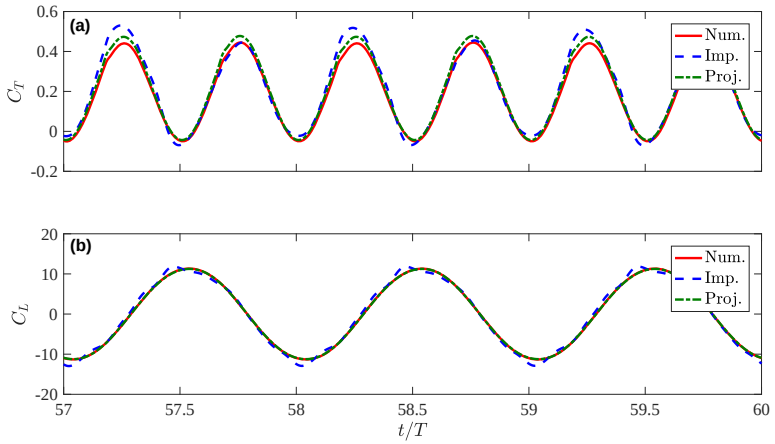

FIG. 6: Comparison of $C_T(t)$ (a) and $C_L(t)$ (b) during three periods, well after a periodic state has been reached, computed with (5) (Num.), with (11) (Imp.), and with (21) (Proj.) for $h_0 = 0.05$, $k = 6$ and $Re = 20\,000$. The size of the control volume V_c used in (11) and (21) corresponds to $r = l = 10$.

V. RESULTS AND DISCUSSION

A. Validation of the vortex force formulas

Before comparing the performance of the force approximations (13), (24) and (27), it is convenient to validate the exact expressions (11) and (21) with the numerical results from the standard force expression (5), already validated with experimental results above.

Figure 6 compares the results from the standard aerodynamic force expression (5), the impulse formula (11) and the projection expression (21) for $h_0 = 0.05$, $k = 6$ and $Re = 20\,000$. All the terms in (11) and (21) (including the viscous ones, proportional to Re^{-1}) are computed in a control volume V_c like that sketched in Fig. 1 with $r = 10$ and $l = 10$ (i.e., S_E located ten chord lengths downstream from the trailing edge). For this value $k = 6$ the flow becomes periodic with period $T = \pi/k$, and the temporal evolutions of C_T and C_L are plotted in Fig. 6 during three whole periods well after a periodic state has been reached starting from rest. The curves $C_T(t)$ and $C_L(t)$ practically coincide, within numerical errors, when computed with the three quite different approaches. It is particularly remarkable the excellent agreement in C_L when computed with the standard force expression (5) and the projection formula (21).

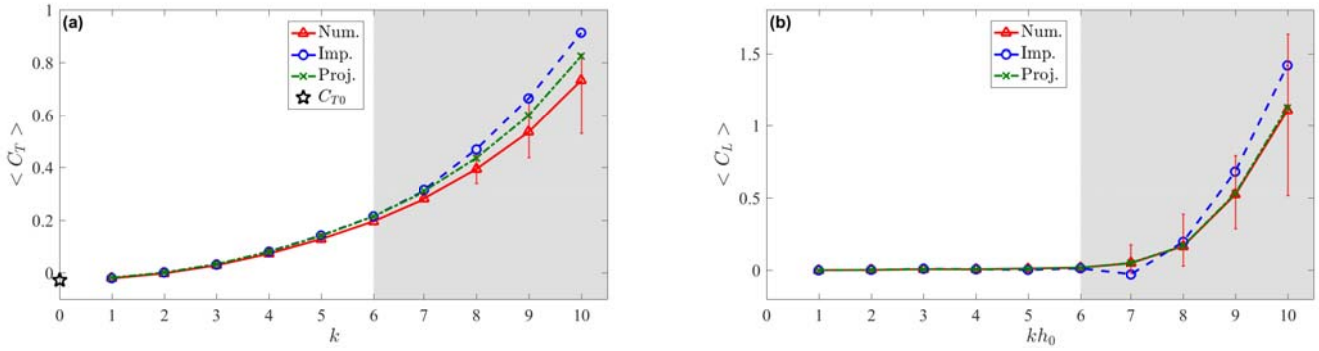

FIG. 7: Averaged values of C_T (a) and C_L (b) vs. k for $Re = 20\,000$ and $h_0 = 0.05$, computed with (5) (Num.), with (11) (Imp.), and with (21) (Proj.). The error bars are for the values computed with (5) when the flow is not longer periodic (shaded area).

The averaged quantities $< C_L >$ and $< C_T >$ as functions of k computed with the three formulations are plotted in Fig. 7. Like in Figs. 3-4, the flow becomes aperiodic for $kh_0 \gtrsim 0.3$ ($k \gtrsim 6$ in this case), which is marked with a shaded area in the figure, including error bars for the averaged values as discussed at the

end of §II. It is interesting to note that in all the computed cases in the present work the transition to an aperiodic flow, which is a consequence of a chaotic wake, occurs approximately at the same value of $kh_0 \simeq 0.3$, corresponding to a Strouhal number $St \simeq 0.9$, in accordance with some previous works at different Reynolds numbers [35]. For $k \lesssim 6$ the results from the three formulations practically coincide. For k larger than 6, the fluctuations in the mean values, especially for C_L, become quite large, as indicated by the errors bars, and the agreement between the mean values computed with three force formulations becomes poorer. Again, it is remarkable the agreement in $< C_L >$ when computed with the standard force expression (5) and the projection formula (21), even for $k > 6$.

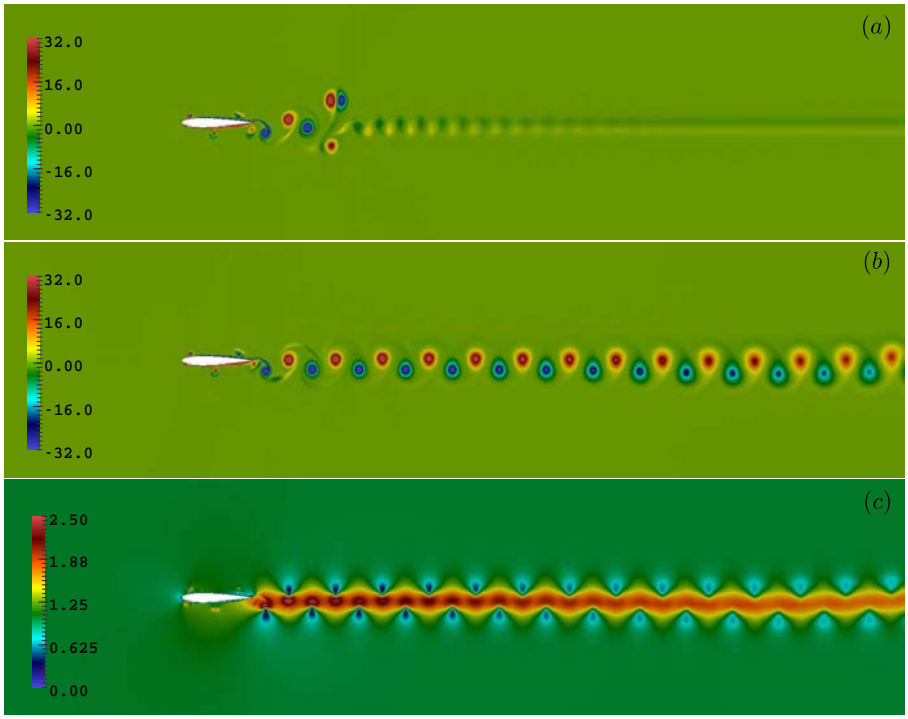

FIG. 8: Vorticity fields at $t/T = 2.75$ (a) and $t/T = 50.75$ (b), and mean velocity $|\mathbf{v}|$ field at $t/T = 50.75$ (c), of the flow starting at $t = 0$ with a periodic developed wake from the steady case, for $h_0 = 0.05$, $Re = 20\,000$ and $k = 6$. S_E is located 10 chord lengths downstream from the trailing edge, but the control volume is not shown in its entirety.

B. Analysis of the vortex impulse formulation

We analyze first the relative importance of the different (non-viscous) terms of the impulse formulation (13)-(16) in two different situations: at the initial stages of the motion when the wake has not reached yet the exit surface S_E of the control volume V_c, and when a permanent state has been reached after a long time, with a periodic wake exiting through S_E. These two regimes are visualized in Figs. 8 (a) and (b) by the vorticity fields at $t/T = 2.75$ and $t/T = 50.75$, respectively, in the reference case with reduced frequency $k = 6$ (all the cases analyzed are for $h_0 = 0.05$ and $Re = 20\,000$). S_E is taken 10 chord lengths downstream from the trailing edge.

As shown in Figs. 9 and 10, the agreement between $C_T(t)$ and $C_L(t)$ computed with the impulse approximation (13)-(16) [i.e., the force expression (11) without the last viscous term and substituting S_e by S_E in the third term] and the "exact" numerical solution from (5) is quite remarkable, especially for C_L. But there is a fundamental difference between the two cases: for t/T around 3 (Fig. 9), when the wake is still far from the exit S_E, the only significant term in the force (13) is the impulse term $\mathbf{F}_I$ (15), while for $t/T = 50$, well after the wake has exited the control volume through S_E, the term $\mathbf{F}_{oE}$ (and $\mathbf{F}_v$ for C_T) is as important as the impulse term $\mathbf{F}_I$. In fact, in this second case, the contributions from $\mathbf{F}_I$ and $\mathbf{F}_{oE}$ to C_L are much larger, in absolute values, than $|C_L|$ [Fig. 10(b)], but they almost cancel each order to produce a quite accurate approximation for C_L, being critical the precision in calculating these terms. The same can be said for C_T in this second case [Fig. 10(a)], but including now a third significant term from the vortex force $\mathbf{F}_v$, and with partial contributions from $\mathbf{F}_I$ and $\mathbf{F}_{oE}$ not so much larger than the total $|C_T|$.

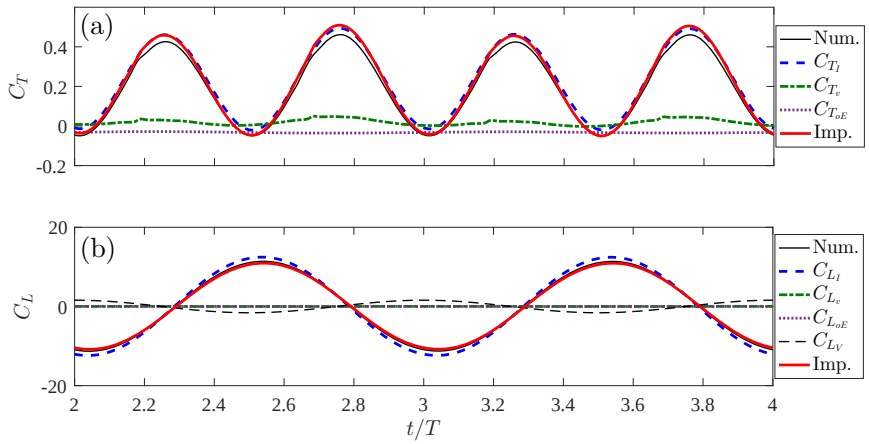

FIG. 9: Comparison of $C_T(t)$ (a) and $C_L(t)$ (b) along two periods around $t/T = 2$ [corresponding to the flow depicted in Fig. 8(a)] computed numerically using (5) (Num.) with the results from the Impulse formulation (13)-(16) (Imp.) and their four components from $\mathbf{F}_v$, $\mathbf{F}_I$, $\mathbf{F}_{oE}$ and $\mathbf{F}_V$ (the last one vanishes for C_T). $h_0 = 0.05$, $Re = 20000$ and $k = 6$. S_E is located 10 chord lengths downstream from the trailing edge.

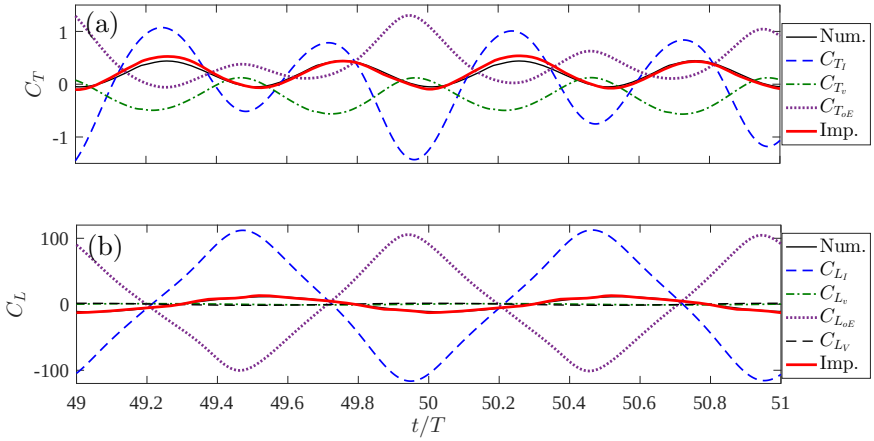

FIG. 10: As in Fig. 9 but for two periods around $t/T = 50$, corresponding to the flow depicted in Fig. 8(b).

To better appreciate this transition in the contributions of the different terms of (13) to C_T and C_L, Fig. 11 shows the temporal evolutions of these force coefficients around the instant $t/T = 17$ when the airfoil's wake reaches S_E. At this instant, the amplitude of the oscillations of $\mathbf{F}_I$ and $\mathbf{F}_{oE}$ increase abruptly, especially for the horizontal component C_T, but they almost cancel each other to produce a very good approximation to the total aerodynamic force all along the transition as well.

Thus, once the wake exits the control volume, the impulse force $\mathbf{F}_I$ is a very poor and useless approximation to the aerodynamic force, which has to be complemented with the other terms in (13), especially $\mathbf{F}_{oE}$, to produce a good force approximation. Only when the entire wake is inside V_c, as in the starting flow of Fig. 8(a), or if one uses a huge control volume V_c, $\mathbf{F}_I$ is a good approximation to the force. These are bad news for using the impulse approximation with experimental data in oscillating flows like the present one for flapping airfoils in forward flight, because a small error in computing either $\mathbf{F}_I$ or $\mathbf{F}_{oE}$ from the experimental data in the permanent regime will generate a large error in the total force, especially for C_T. It is however a good method for computing forces from experimental data in hovering flapping airfoils, because the entire vortex system generated by the oscillating airfoil remains inside a manageable control volume.

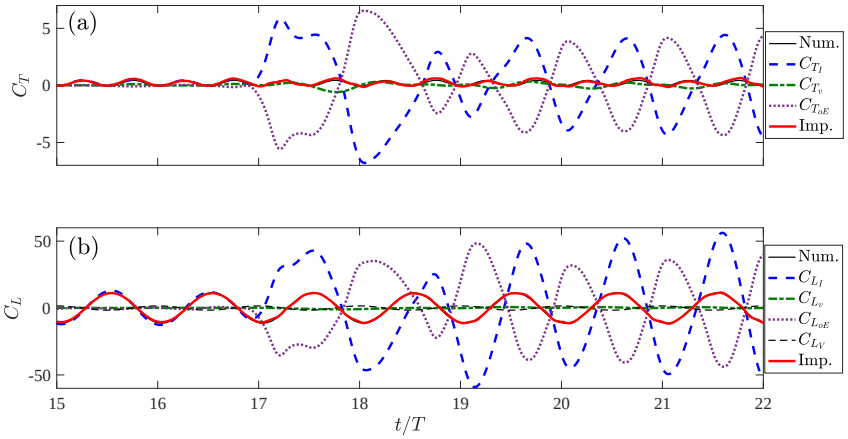

FIG. 11: As in Fig. 9 but for several cycles around the transition time $t/T = 17$, when the wake reaches S_E. Note that the curves 'Num.' and 'Imp.' practically coincide for all time.

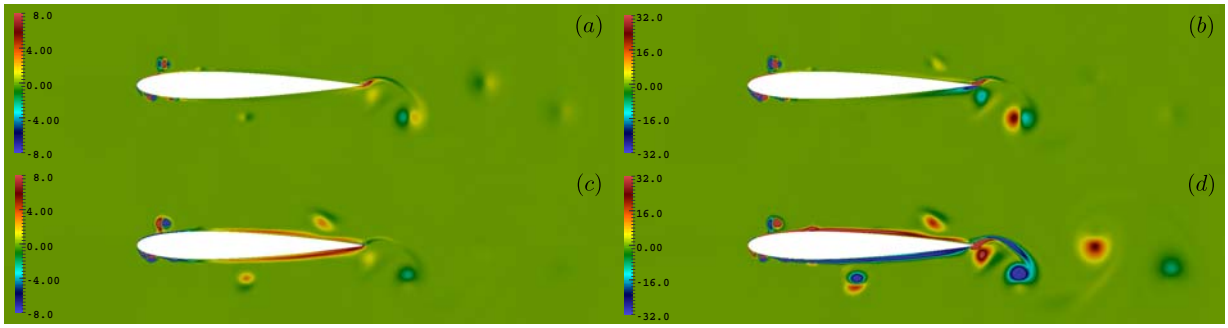

FIG. 12: Density fields of thrust (left) and lift (right) corresponding to the different terms of $\mathbf{F}_{vf}$ in (26): $\omega v_z(\partial\varphi_x/\partial x)$ (a), $\omega v_z(\partial\varphi_z/\partial x)$ (b), $-\omega v_x(\partial\varphi_x/\partial z)$ (c), $-\omega v_x(\partial\varphi_z/\partial z)$ (d). $t/T = 50.75$ (mid upstroke) for $h_0 = 0.05$, $Re = 20000$ and $k = 6$.

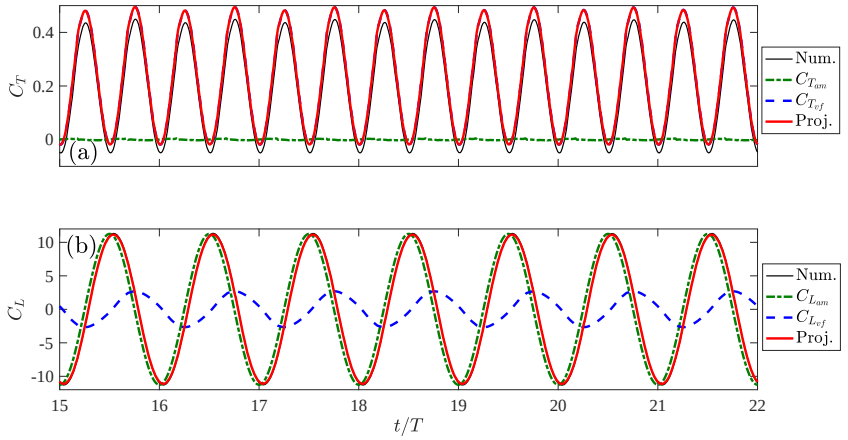

FIG. 13: Comparison of $C_T(t)$ (a) and $C_L(t)$ (b) along several periods around $t/T = 17$ (corresponding to the instant when the airfoil's wake reaches S_E) computed numerically using (5) (Num.) with the results from the projection formulation (24)-(26) (Proj.), and their two components from $\mathbf{F}_{am}$ and $\mathbf{F}_{vf}$. $h_0 = 0.05$, $Re = 20000$ and $k = 6$. S_E is located 10 chord lengths downstream from the trailing edge.

C. Analysis of the projection formulation

The above commented problem occurring in the vortex impulse formulation does not takes place when using Chang's projection formulation [4], because the auxiliary potential function (22) eliminates the influence on the force of any vortex which is not sufficiently close to the flapping airfoil (see Fig. 5). This is better appreciated in Fig. 12, where the different terms of $\mathbf{F}_{vf}$ in (26) are plotted for a given instant.

Thus, as it is observed in Fig. 13, the force computed with just the two contributions in (24)-(26) is a very good approximation for any time, before and after the wake reaches S_E at $t/T \simeq 17$. What happens near S_E has no effect on the force computed with the projection formulation. For the present heaving motion with $k = 6$, only the vortex component $C_{T_{vf}}$ is relevant for C_T, while most of C_L comes from the added-mass component $C_{L_{am}}$, as expected. Note that the vertical component computed with (24)-(26) practically coincides with the exact numerical one from (5) [Fig. 13(b)]. The only drawback of the method is that one has to compute previously the auxiliary potential function (22), but this is quite easily done for any airfoil shape and it has to be computed just once.

D. Analysis of the integral momentum approximation

Contrary to the impulse formulation discussed above, the integral momentum approximation (27)-(29) is not useful for the initial stages of the flow when the wake has not reached S_E yet, because then the wake contribution $\mathbf{F}_{vE}$ given by (29), which is the most significant one for C_T, vanishes. But, as shown in Fig. 14, even for the flow conditions of Fig. 8, when t/T is around 50 and the wake has already crossed S_E, the integral momentum force approximation (27)-(29) is a rather poor approximation to both C_T and C_L for the present S_E located 10 chord lengths downstream from the trailing edge. Note that all C_L comes practically from the volume contribution $\mathbf{F}_{tv}$ while the more important contribution to C_T comes from the wake component $\mathbf{F}_{vE}$, as expected.

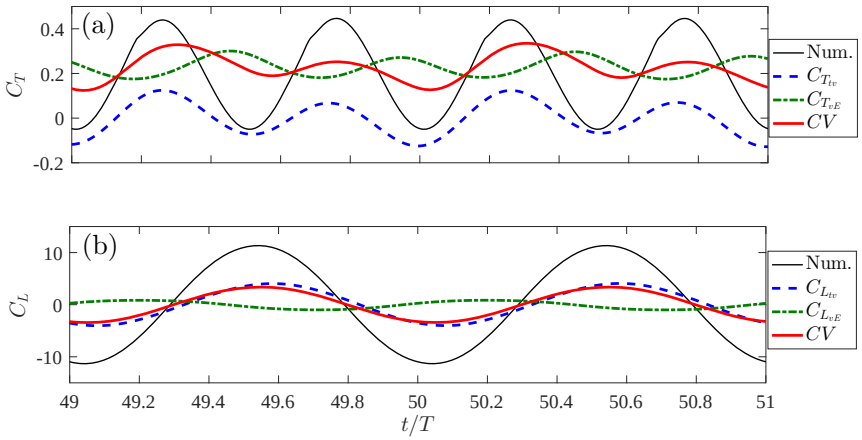

FIG. 14: Comparison of $C_T(t)$ (a) and $C_L(t)$ (b) along two periods around $t/T = 50$ computed numerically using (5) (Num.) with the results from the integral momentum approximation in the control volume (CV) and their two components from $\mathbf{F}_{tv}$ and $\mathbf{F}_{vE}$. $h_0 = 0.05$, $Re = 20000$ and $k = 6$. S_E is located 10 chord lengths downstream from the trailing edge.

This poor performance is somewhat improved when the exit surface S_E is approached to the airfoil. Figure 15 shows the results for the same case of Fig. 14 but with S_E located just 3 chord lengths downstream from the trailing edge. The contribution of the exit wake to the thrust, $C_{T_{vE}}$, is much larger, but the other (volumetric) component of C_T, and the two components of C_L, are practically unaffected by the position of S_E. This is explained by the decay of the wake intensity as one moves downstream from the trailing edge [see Figs. 8(b) and (c)], and the fact that almost all C_T comes from $C_{T_{vE}}$. If this term is computed with S_E located between about 1 and 7 chord lengths, the results are practically the same, now over-estimating C_T, as already noted by Bohl and Koochesfahani [36]. These authors showed that this performance can be improved by using a more complete control volume analysis that takes into account the streamwise velocity fluctuations and the pressure term on S_E, but at the cost of greatly complicating the formulation.

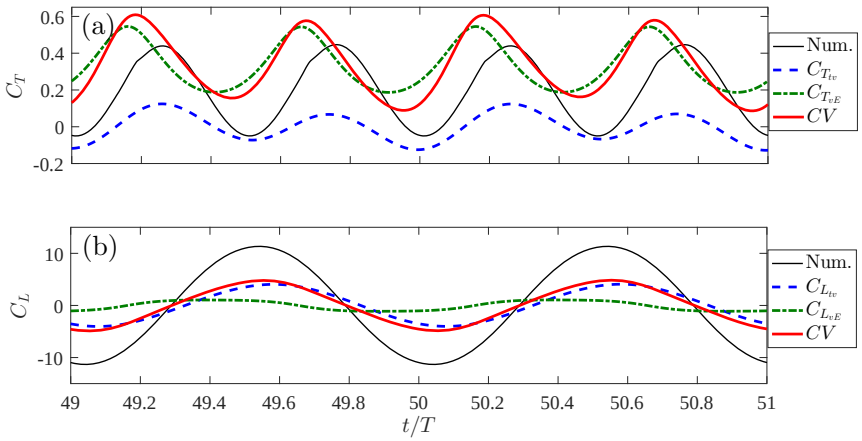

FIG. 15: As in Fig. 14, but for S_E located 3 chord lengths downstream from the trailing edge.

Thus, the results from the integral volume formulation are rather poor and too much dependent on the exit surface S_E of the control volume. In contrast, the other two approaches are practically independent on the location of S_E and much more accurate.

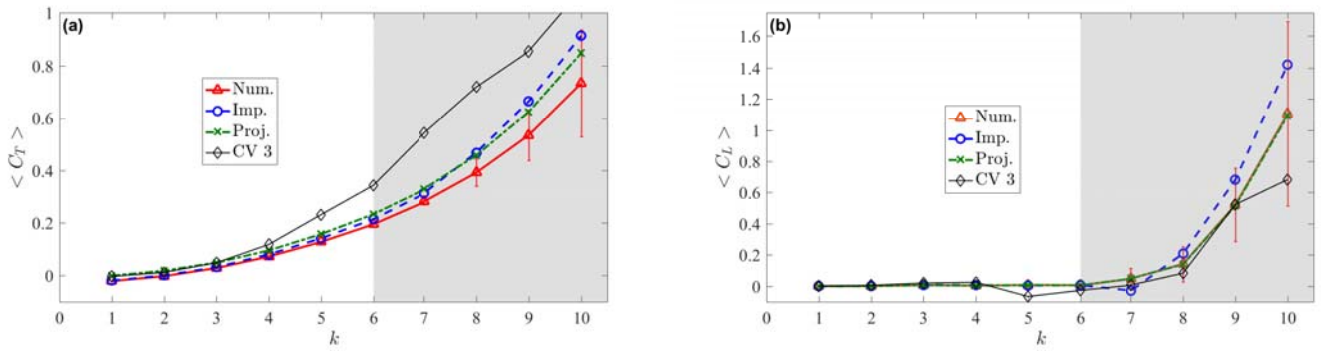

FIG. 16: Averaged values of C_T (a) and C_L (b) vs. k for $Re = 20\,000$ and $h_0 = 0.05$, computed with (5) (Num.), with the impulse/Lamb approximation (13) (Imp.), with the projection approximation (24) (Proj.), and with the integral momentum approximation (27) when S_E is located three chords length downstream from the leading edge (CV 3). The error bars are for the values computed with (5) when the flow is not longer periodic (shaded area).

E. Comparison of the averaged results for different frequencies

As a summary of the results for other values of the reduced frequency k, Fig. 16 shows a comparison of the averaged values of $< C_T >$ and $< C_L >$ as k increases. Both, the impulse/Lamb approximation (13) and the projection approximation (24) agree quite well with the exact numerical results, especially while the flow remains periodic for $k \lesssim 6$: $< C_L >$ computed from these two approximations is almost indistinguishable from the exact results for $k \leq 6$, while the small difference in $< C_T >$ for $k \leq 6$ is basically the quasi-static drag C_{T0} [see Fig. 7(a)], associated to the neglected terms in (11) and (21). On the contrary, the integral volume approximation (27) gives poorer results, greatly over-estimating $< C_T >$ even for $k \leq 6$.

VI. CONCLUSION

We have compared the performance of two different vortex force formulations for predicting the aerodynamic forces (thrust and lift) on an oscillating 2D foil at high Reynolds numbers. One formulation is based on the

vortical impulse and, since it is applied to a large, but finite, volume, it contains additional terms in relation to Wu's formula [1] (i.e., in addition to the temporal derivative of the impulse in the total volume , including the solid volume, and the term related to the acceleration of the solid body) [31]: a term corresponding to Lamb's vector integrated in the fluid volume, and a term associated to the flux of vorticity out of the control volume (apart from the viscous term negligible for high Reynolds numbers). The other method, based on Chang's projection formula [4], contains only two terms (apart from a viscous term negligible for high Reynolds numbers): an added-mass term identical to that given by the potential flow theory, and another one also associated to Lamb's vector integral in the fluid volume, but now conveniently weighted by the projection function. We also compare these two formulations with the traditional force expression coming from plain momentum conservation in the control volume.

For a flapping foil in forward flight it is shown that the most convenient formulation to compute forces from given velocity and vorticity fields is Chang's projection formulation. Its only drawback is the necessity of computing previously the vector projection function. But this function only depends on the solid shape and, once computed, can be used for any flow condition to compute the added-mass force term, which only depends on the solid motion, and to concentrate the relevant vortical (Lamb's vector) contributions to the aerodynamic vortex force near the solid body, so that the results are practically independent on the size of the control volume used. In the example considered here, practically all the thrust force came from Lamb's vector projection term, while almost all the lift was added-mass force.

In the case of the vortical impulse formulation applied to a flapping foil in forward flight or swimming, the impulse term is as important as the term accounting for the wake vorticity flux exiting the control volume, and they almost cancel each other. Although the net result is as accurate as the projection formulation, in practice, when using experimental data, any small imprecision in the numerical computation of these volume or surface integrals of the vorticity and velocity fields may produce large error in the computed force. To complicate matters a little bit more, Lamb's vector contribution is also important. In fact, it is of the same order as the force computed from the three terms, with the additional disadvantage that Lamb's vector is no longer weighted near the solid body as in the equivalent projection term, so that all the vorticity distributed inside the control volume contributes equally to the force. Only when vorticity does not exit the control volume, like, for instance, during the starting motion of the foil, or in a hovering flapping foil, the impulse formulation is as efficient as the projection formulation to compute forces, because almost all the force comes then from the impulse term. In these cases the impulse formulation may even have some advantages because one avoids computing the projection function. It can also be more convenient for just estimating forces when a few localized vortices are present in the flow, because one may follow the vortices and compute the associated vortical impulse using approximate models [37–40]. Although the results have been obtained here for a simple heaving foil, these general conclusions about the comparative suitability of the two vortex formulations may be clearly applied to more complicated scenarios.

In relation to these two methods, the standard integral momentum method, which is much simpler to implement using experimental data, is quite inaccurate predicting the temporal evolution of both the lift and the thrust forces, largely overestimating the time-averaged thrust.

Acknowledgments

This research has been supported by the *Ministerio de Economía y Competitividad* of Spain Grant No. DPI2016-76151-C2-1-R. The computations were performed in the Picasso Supercomputer at the University of Málaga, a node of the Spanish Supercomputing Network.

[1] J. C. Wu. Theory for the aerodynamic force and moment in viscous flows. *AIAA J.*, 19:432–441, 1981.
[2] J. Lighthill. *An informal introduction to theoretical fluid mechanics*. Clarendon Press, Oxford, 1986.
[3] P.G. Saffman. *Vortex dynamics*. Cambridge University Press, New York, 1992.
[4] C.-C. Chang. Potential flow and forces for the incompressible viscous flow. *Proc. R. Soc. A-Math. Phys. Engng Sci.*, 437:517–525, 1992.
[5] F. Noca, D. Shields, and D. Jeon. A comparison of methods for evaluating time-dependent fluid dynamic forces on bodies, using only velocity fields and their derivatives. *J. Fluids Structures*, 13:551–578, 1999.
[6] J.-Z. Wu, H.-Y. Ma, and M.-D. Zhou. *Vorticity and vortex dynamics*. Springer, Berlin, 2006.
[7] J.-Z. Wu, H.-Y. Ma, and M.-D. Zhou. *Vortical flows*. Springer, Berlin, 2015.
[8] Th. von Kármán and W. R. Sears. Airfoil theory for non-uniform motion. *J. Aeronaut. Sci.*, 5:370–390, 1938.

[9] T. Theodorsen. General theory of aerodynamic instability and the mechanism of flutter. Technical Report TR 496, NACA, 1935.

[10] R. Fernandez-Feria. Linearized propulsion theory of flapping airfoils revisited. *Phys. Rev. Fluids*, 1:084502, 2016.

[11] L. Quartapelle and M. Napolitano. Force and moment in incompressible flows. *AIAA J.*, 21:911–913, 1983.

[12] M. S. Howe. On the force and moment on a body in an incompressible fluid, with application to rigid bodies and bubbles at high and low Reynolds numbers. *Q. Jl. Mech. Appl. Math.*, 48:401–426, 1995.

[13] C.-T. Hsieh, C.-C. Kung, C. C. Chang, and C.-C. Chu. Unsteady aerodynamics of a dragonfly using a simple wing-wing model from the perspective of force decomposition. *J. Fluid Mech.*, 663:233–252, 2010.

[14] G. J. Li and X. Y. Lu. Force and power of flapping plates in a fluid. *J. Fluid Mech.*, 712:598–613, 2012.

[15] J. Kriegseis and D. E. Rival. Vortex force decomposition in the tip region of impulsively-started flat plates. *J. Fluid Mech.*, 756:758–770, 2014.

[16] A. Martín-Alcántara, R. Fernandez-Feria, and E. Sanmiguel-Rojas. Vortex flow structures and interactions for the optimum thrust efficiency of a heaving airfoil at different mean angles of attack. *Phys. Fluids*, 27:073602, 2015.

[17] H. Lamb. *Hydrodynamics*. Dover, New York, 1945.

[18] G. C. Lewin and H. Haj-Hariri. Modelling thrust generation of a two-dimensional heaving airfoil in a viscous flow. *J. Fluid Mech.*, 492:339–362, 2003.

[19] P. Blondeaux, L. Guglielmini, and M. S. Triantafyllou. Chaotic flow generated by an oscillating foil. *AIAA J.*, 43:918–921, 2005.

[20] H. Jasak. *Error Analysis and Estimation for the Finite Volume Method with Applications to Fluid Flows*. PhD thesis, Imperial College, London, 1996.

[21] P. D. Lax and B. Wendroff. Systems of conservation laws. *Comm. Pure Appl. Math.*, 13:217–237, 1960.

[22] J. H. Ferziger and M. Perić. *Computational Methods for Fluid Dynamics*. Springer-Verlag, New York, 2001.

[23] Y. Lian and W. Shyy. Aerodynamics of low Reynolds number plunging airfoil under gusty environment. *AIAA Paper 2007-71*, 2007.

[24] F. M. Bos, D. Lentink, B. W. van Oudheusden, and H. Bijl. Influence of wing kinematics on aerodynamic performance in hovering insect flight. *J. Fluid Mech.*, 594:341–368, 2008.

[25] J. Young and J. C. S. Lai. Mechanisms influencing the efficiency of oscillating airfoil propulsion. *AIAA J.*, 45:1695–1702, 2007.

[26] G. Z. McGowan, K. Granlund, M. V. Ol, A. Gopalarathnam, and J. R. Edwards. Investigations of lift-based pitch-plunge equivalence for airfoils at low Reynolds numbers. *AIAA J.*, 49:1511–1524, 2011.

[27] S. Heathcote and I. Gursul. Flexible flapping airfoil propulsion at low Reynolds numbers. *AIAA J.*, 45:1066–1079, 2007.

[28] I. E. Garrick. Propulsion of a flapping and oscillating airfoil. Technical Report TR 567, NACA, 1936.

[29] A. W. Mackowski and H. K. Williamson. Effect of pivot point location and passive heave on propulsion from a pitching airfoil. *Phys. Rev. Fluids*, 2:013101, 2017.

[30] R. Fernandez-Feria. Note on optimum propulsion of heaving and pitching airfoils from linear potential theory. *J. Fluid Mech.*, 826:781–796, 2017.

[31] J.-Z. Wu, X.-Y. Lu, and L.-X. Zhuang. Integral force acting on a body due to local flow structures. *J. Fluid Mech.*, 576:265286, 2007.

[32] G. K. Batchelor. *An introduction to fluid dynamics*. Cambridge University Press, 1967.

[33] M. Moriche, O. Flores, and M. Garcia-Villalba. On the aerodynamic forces on heaving and pitching airfoils at low Reynolds number. *J. Fluid Mech.*, 828:395–423, 2017.

[34] J. N. Newman. *Marine hydrodynamics*. The MIT Press, Cambridge (MA), 1977.

[35] J. Deng, L. Sun, L. Teng, D. Pan, and X. Shao. The correlation between wake transition and propulsive efficiency of a flapping foil: A numerical study. *Phys. Fluids*, 28:094101, 2016.

[36] D. G. Bohl and M. M. Koochesfahani. MTV measurements of the vortical field in the wake of an airfoil oscillating at high reduced frequency. *J. Fluid Mech.*, 620:63–88, 2009.

[37] A. A. Tchieu and A. Leonard. A discrete-vortex model for the arbitrary motion of a thin airfoil with fluidic control. *J. Fluids Structures*, 27:680–693, 2011.

[38] C. Wang and J. D. Eldredge. Low-order phenomenological modeling of leading-edge vortex formation. *Theor. Comput. Fluid Dyn.*, 27:577–598, 2013.

[39] C. W. Pitt Ford and H. Babinsky. Lift and the leading-edge vortex. *J. Fluid Mech.*, 720:280–313, 2013.

[40] R. Fernandez-Feria and J. Alaminos-Quesada. Unsteady thrust, lift and moment of a two-dimensional flapping thin airfoil in the presence of leading-edge vortices: a first approximation from linear potential theory. *J. Fluid Mech.*, 851:344–373, 2018.